お茶の水女子大学自然科学報告　第71巻　第1号、第2号
Natural Science Report, Ochanomizu University, Vol. 71, No. 1, No. 2（2021）

# Numerical simulation of flow around Wing-In-Surface-Effect under various conditions

**Tetuya Kawamura, Akari Oniiwa and Aya Saito**

**(Received August 31, 2019)**

**Abstract**

Lift of a wing becomes larger while induced drag becomes smaller when distance between a wing and the ground or sea surface becomes smaller. This phenomenon is known as the ground effect or surface effect. WISE (Wing in surface effect) is a vehicle flying near the sea to utilize this effect and to improve the efficiency of flight. In this study, numerical simulation is carried out to estimate the surface effect on the vehicle under various conditions such as attack angle, distance from the surface to see their effect on the L/D (ratio of lift to drag). We also change the shape of the surface caused by the wave assuming real sea surface and investigate its effect on the flow field and L/D.

## 1. Introduction

People and supplies traveling to and from remote islands are mainly transported by plane and ship, but the former is limited in load capacity and the latter is limited in moving speed, so more efficient means of transportation is required. One of the possible means is a WISE (wing in surface effect), which is a vehicle that uses surface effects to increase lift and reduce induced drag by flying near the sea surface [1].

WISE is mainly researched and developed in Russia and China, but many are improved airplanes. Therefore, the shape of the wing is similar to that of an airplane. On the other hand, one of the authors focused on the small WISE and was involved in the development of a new airframe with wings that were bent into a wing shape. The aerodynamic properties of such a hollow wing are quite different from those of a typical wing shape. Although it did not reach practical use, there is a single seat μ-sky 1 and a two seats μ-sky 2 in the prototype of new WISE jointly developed by Mitsubishi Heavy Industries and Tottori University in the early 1990s [2), 3)].

There are several papers on the surface effect and stability of general wing shapes of WISE [4), 5), 6)]. However, there are few studies on our special WISE having the characteristic shape.

In order to propose conditions for our WISE to fly efficiently, the flow around it should be numerically simulated using the three-dimensional Navier-Stokes equation estimating the influence of the control parameters such as the distance from the water surface and the angle of attack on the flow field and the L/D (ratio of lift to drag). Moreover, there are waves in the actual sea surface and it cannot be regarded as a plane in many cases.

Therefore, in this paper, we also conduct the simulation considering the unevenness of the sea surface due to the wave to see its influence on the flow field and L/D.

## 2. Numerical Method

### 2-1 Basic equations

Since the flow at the flight speed of WISE can be regarded as an incompressible fluid, the continuity equation (1) and the Navier-Stokes equation (2) are used as the basic equations.

$$\frac{\partial u}{\partial x}+\frac{\partial v}{\partial y}+\frac{\partial w}{\partial z}=0 \tag{1}$$

$$\left.\begin{aligned}
&\frac{\partial u}{\partial t}+u\frac{\partial u}{\partial x}+v\frac{\partial u}{\partial y}+w\frac{\partial u}{\partial z}=-\frac{\partial P}{\partial x}+\frac{1}{\mathrm{Re}}\left(\frac{\partial^2 u}{\partial x^2}+\frac{\partial^2 u}{\partial y^2}+\frac{\partial^2 u}{\partial z^2}\right)\\
&\frac{\partial v}{\partial t}+u\frac{\partial v}{\partial x}+v\frac{\partial v}{\partial y}+w\frac{\partial v}{\partial z}=-\frac{\partial P}{\partial y}+\frac{1}{\mathrm{Re}}\left(\frac{\partial^2 v}{\partial x^2}+\frac{\partial^2 v}{\partial y^2}+\frac{\partial^2 v}{\partial z^2}\right)\\
&\frac{\partial w}{\partial t}+u\frac{\partial w}{\partial x}+v\frac{\partial w}{\partial y}+w\frac{\partial w}{\partial z}=-\frac{\partial P}{\partial z}+\frac{1}{\mathrm{Re}}\left(\frac{\partial^2 w}{\partial x^2}+\frac{\partial^2 w}{\partial y^2}+\frac{\partial^2 w}{\partial z^2}\right)
\end{aligned}\right\} \tag{2}$$

### 2-2 Numerical Method

We solve the above equations using the fractional step method [7]. Third order upwind difference is used to approximate the non-linear terms of the Navier-Stokes equation to perform stable computation even at high Reynolds number. Other terms in the equations are approximated by the second order central difference.

With $\Delta t = 0.001$, we calculated up to 20 in dimensionless time.

## 3. Conditions of computations

### 3-1 Model of WISE

In this research, μ-sky 1 is assumed to be analyzed. Fig.1 is a conceptual figure of μ-sky1. A simplified model of it without a center body and a horizontal tail is created, and three-dimensional numerical simulation is carried out. The shape of the upper side of the wing is basically NACA0012 type but the thickness is increased by a factor 2. The airframe is hollow and the aspect ratio is 1. It has end-plates attached to both ends of wing in the span direction.

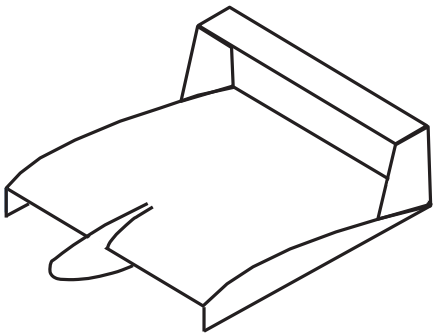

Fig. 1 Sketch of WISE

In absent of waves, the distance (= $d$) between the trailing

edge of the wing and the sea surface is changed from 1/20 to 1/5 of the chord length C and the attack angle α is changed from 0 to 15 degrees. On the other hand, in the presence of waves they are fixed to 1/10 of the chord length and 10 degree respectively.

The wave is expressed as a traveling wave with the speed of the WISE because the coordinate system moving with WISE is used. In this case, the wave is assumed to be a one-dimensional sinusoidal wave with a wave front perpendicular to the WISE. The Reynolds number is set to 2000 in consideration of the grid resolution.

### 3-2 Grid around WISE

The computational domain including WISE is divided into two as shown in Fig. 2. The grid is along the wing, and the grid number is 181 × 41 × 31 (=X × Y × Z) in region 1 of the figure, and 119 × 31 × 31 (=X × Y × Z) in region 2 (Fig. 2, 3). In addition, the size of grids is made finer as it gets closer to the wing (Fig. 3). Since the shape of sea surface changes with time, grids are generated step by step.

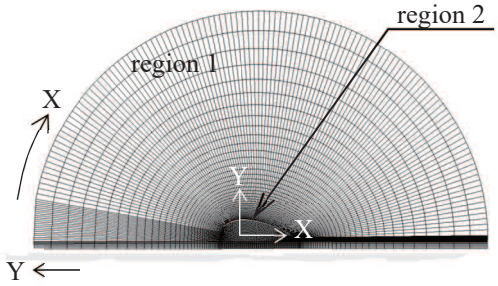


Fig. 2 Grid (side view)

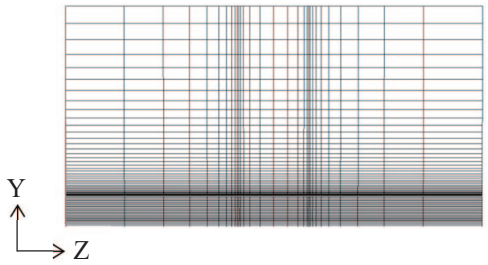


Fig. 3 Grid (front view)

### 3-3 Boundary conditions

The boundary conditions are as shown in the figure (Fig. 4, 5). The average value of the grid points on both sides is used along the joint line between two regions (Fig.5).

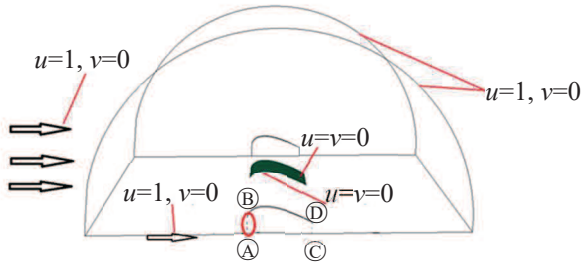


Fig. 4 Schematic of boundary conditions

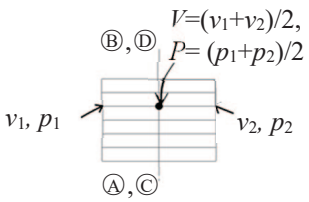


Fig. 5 Treatment on the joint plane

## 4. Results and discussions

### 4-1 Effect of distance from sea surface

The pressure and the velocity vector of the flow when the distance to the sea surface is changed are shown in the following figures (Fig. 6 - 8). The lift and drag ratio (L/D) in each case is shown in Table 1 as well as in Fig.9 in which the change of L/D by the distance is shown. Note that two types of the cross section are used to visualize flow field, one is the symmetrical plane parallel to XY plane (side view) and the other is center plane of span direction parallel o YZ plane (rear view).

The smaller value of d makes the larger difference in pressure between the upper and lower surfaces of the wing. The region of high velocity due to large pressure difference is observed near the trailing edge. If d is small, the vortex is observed in the region between leading edge of the wing and sea surface. However, the vortex weakens as d increases. It is also clear that the tip vortices are generated in the cross section in the span direction. It is also understood from the table of computational results that the lift-drag ratio decreases as the distance from the sea surface increases.

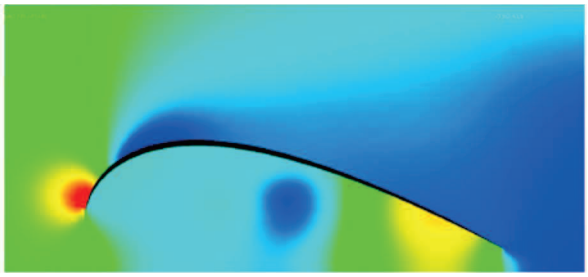

(a) Pressure distribution in the center plane (side view)

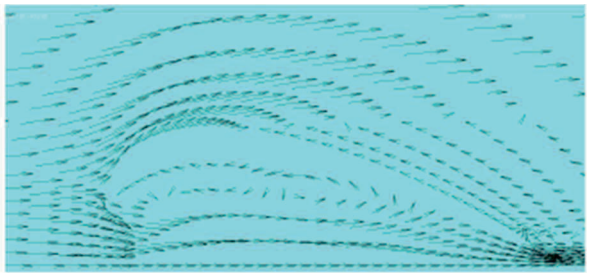

(b) Velocity vectors in the center plane (side view)

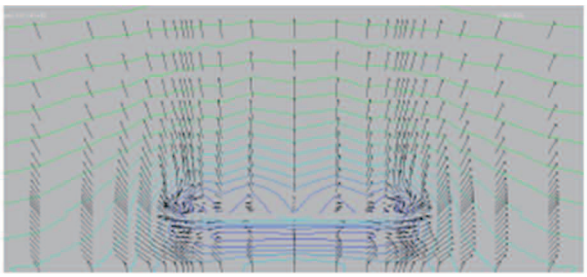

(c) Velocity vectors and pressure contours in the plane of span direction showing trailing vortices (rear view)

Fig. 6 Calculation results in $d$= 0.05

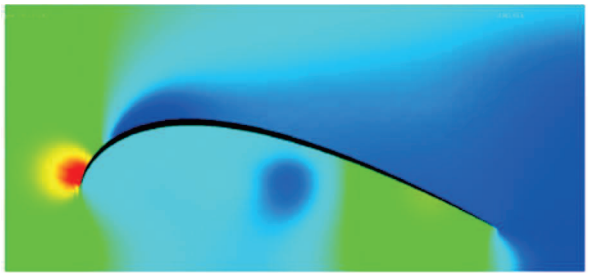

(a) Pressure distribution in the center plane (side view)

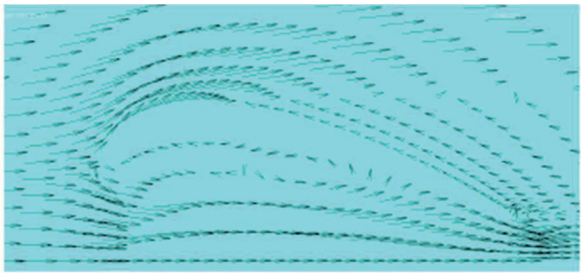

(b) Velocity vectors in the center plane (side view)

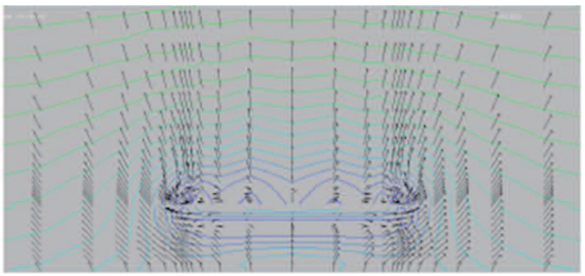

(c) Velocity vectors and pressure contours in the plane of span direction showing trailing vortices (rear view)

Fig. 7 Calculation results in $d$= 0.1

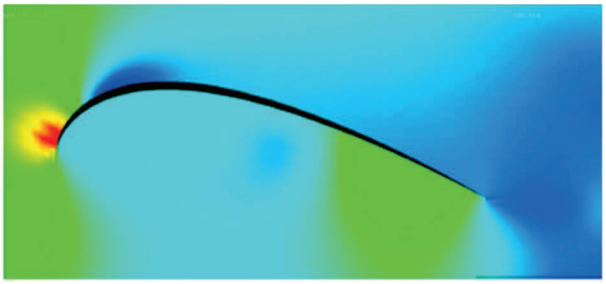

(a) Pressure distribution in the center plane (side view)

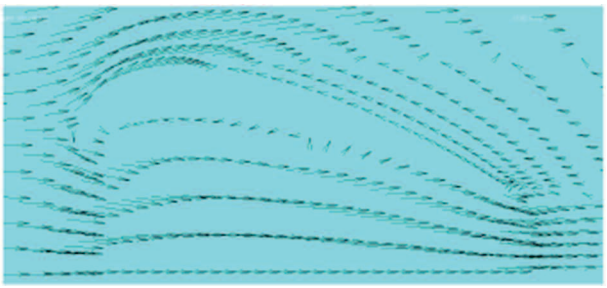

(b) Velocity vectors in the center plane (side view)

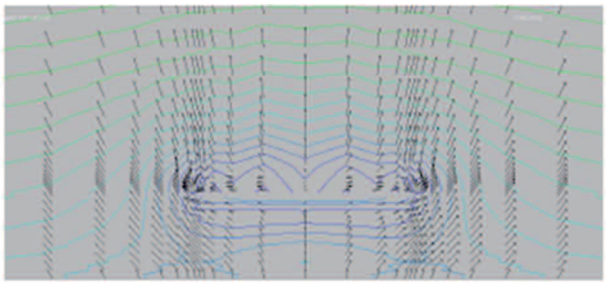

(c) Velocity vectors and pressure contours in the plane of span direction showing trailing vortices (rear view)

Fig. 8 Calculation results in $d$=0.2

Table1 Ratio of lift to drag (L/D) for distance from the ground ($d$)

| $d$ | 0.05 | 0.1 | 0.2 |
|---|---|---|---|
| L / D | 1.73 | 1.55 | 1.36 |

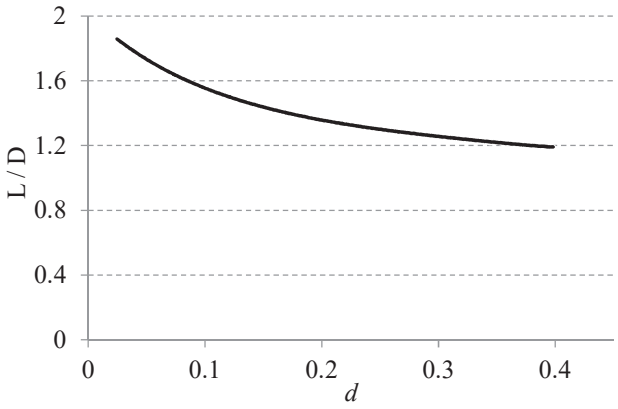


Fig. 9 Ratio of lift to drag (L/D) profile for distance from the ground ($d$)

From these results, the closer the surface to the water, the better the efficiency, but in practice there is also the influence of waves on the sea. These are discussed in section 4.3.

4-2 Effect of attack angle

The pressure and velocity vectors when the angle of attack is changed are shown in the following figures (Fig. 10 - 12). Lift and drag ratio L/D in each case is shown in Table 2. Also, they are plotted in Fig. 13. Note that the cut section is the same as in Section 4.1. As $\alpha$ increase, the pressure on the lower surface of the wing increases, and it can be seen that a large separation vortex is created from the leading edge of the lower surface of the wing due to the air flow from the leading edge. Also, looking at the cross section cut in the span direction (rear view), the tip vortices flowing from the lower surface to the upper surface of the wing become stronger as α increase. From this, as the angle of attack increases, the lift-to-drag ratio L/D increases, however, it can be seen that the L/D decreases as it becomes too large.

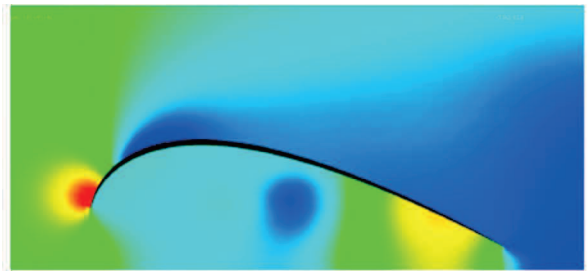

(a) Pressure distribution in the center plane (side view)

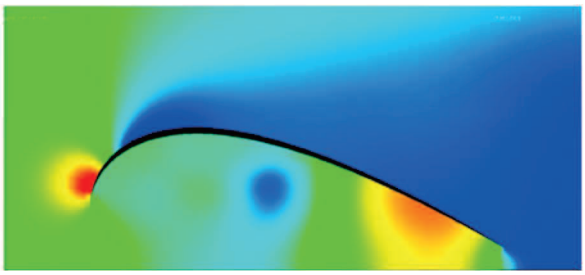

(a) Pressure distribution in the center plane (side view)

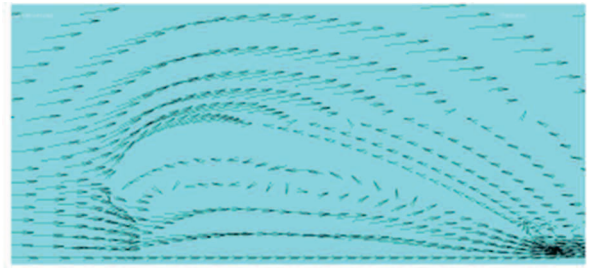

(b) Velocity vectors in the center plane (side view)

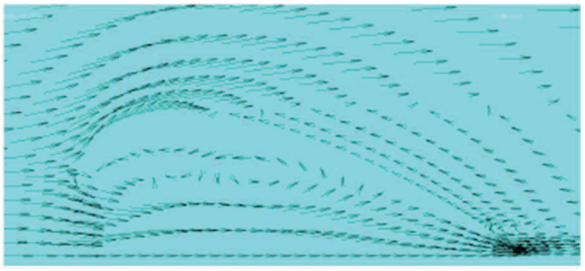

(b) Velocity vectors in the center plane (side view)

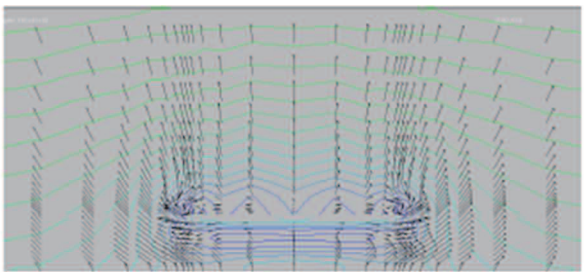

(c) Velocity vectors and pressure contours in the plane of span direction showing trailing vortices (rear view)

Fig. 10 Calculation results in $\alpha = 5$

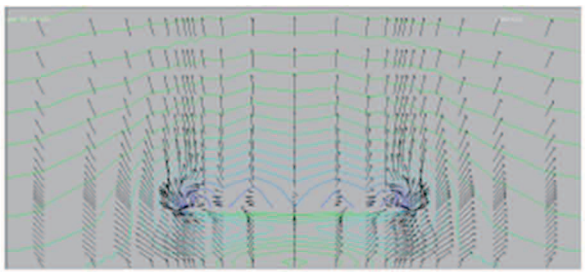

(c) Velocity vectors and pressure contours in the plane of span direction showing trailing vortices (rear view)

Fig. 11 Calculation results in $\alpha = 7$

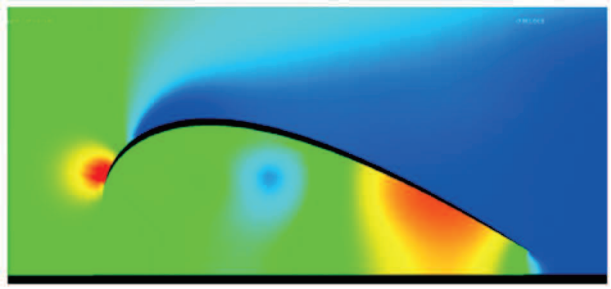

(a) Pressure distribution in the center plane (side view)

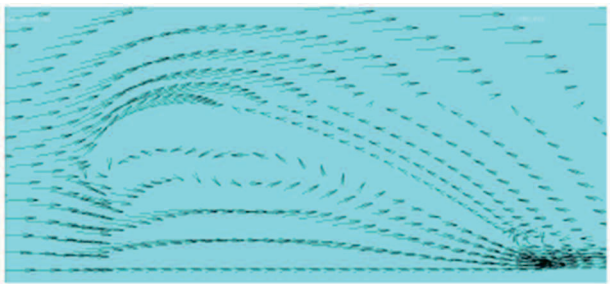

(b) Velocity vectors in the center plane (side view)

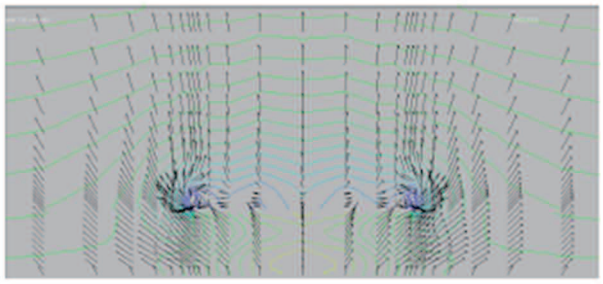

(c) Velocity vectors and pressure contours in the plane of span direction showing trailing vortices (rear view)

Fig. 12 Calculation results in $\alpha = 9$

Table2 Ratio of lift to drag (L/D) for attack angle ($\alpha$)

| $\alpha$ | 5 | 7 | 9 |
|---|---|---|---|
| L / D | 1.73 | 2.00 | 2.14 |

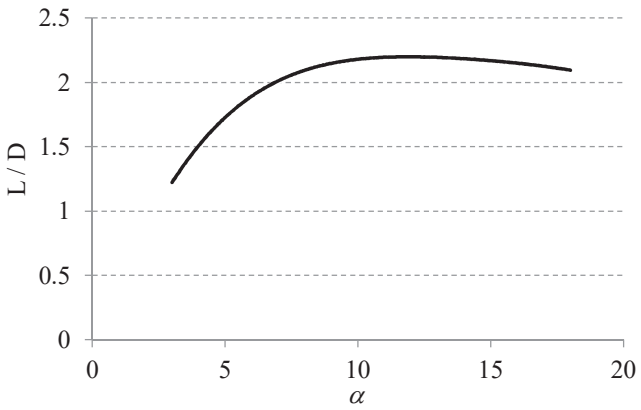


Fig. 13 Ratio of lift to drag (L/D) profile for attack angle ($\alpha$)

4-3 Effect of the sea wave

The computations are carried out for wavelength of the traveling wave being 4C, 2C, and C where C is the chord length of the wing. The angle of attack is fixed to 10 degree and the average distance between the trailing edge and the sea surface is fixed to 0.1 C. The wave amplitude is mainly 0.05C, so the distance between the trailing edge and the sea surface becomes maximum 0.15C and minimum 0.05C. For comparison, we also calculated the amplitude of 0.025 C and 0 (i.e. in the absence of waves).

Fig. 14 shows time history of the lift, drag and L/D in the interval of $t$ = 5 and 7 where the initial conditions have almost no effect. The curves in the figure represent the drag, lift and lift-to-drag ratio L/D in ascending order of values.

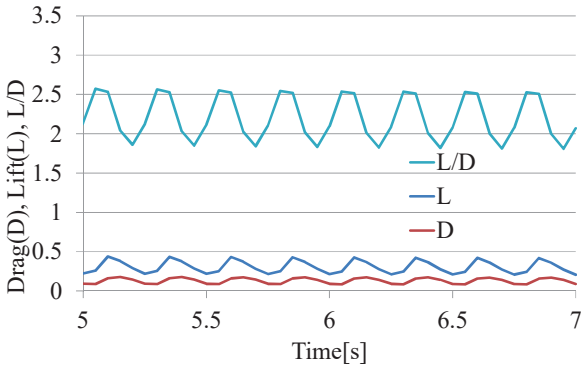


Fig. 14 Time history of Drag(D), Lift(L) and L/D

It can be seen that these curves are wavy in agreement with the wave period ($T$ = 0.25). In addition, it can be seen that the drag and lift are in phase. The waveform of the curve is biased to the left and deviates from the traveling wave (sinusoidal wave), which is caused by the fact that the shape of the wing is not flat. On the other hand, the curve of the lift and drag ratio L/D has nearly symmetrical form. It is also clear that the maximum and minimum values are offset from the position of those values of lift and drag.

Fig. 15 shows the pressure distribution in the symmetric cross section at $T$ = 6.0, 6.1, 6.2, 6.3, 6.4 obtained by equally dividing one cycle. They are shaded by using the normalized value based on the maximum and the minimum value. The leading edge of the wing is always at high pressure, but it can be seen that the high pressure part between the wing and the sea surface moves downstream as the wave advances.

In the lower two figures, it is observed that vortices are emitted downward from the leading edge. In addition, the pressure on the upper side of the wing also fluctuates with the pressure fluctuation on the lower side of the wing. It is considered that the flow field reflects the changes in the distance between the wing and the sea surface that causes the change of the volume of the enclosed space.

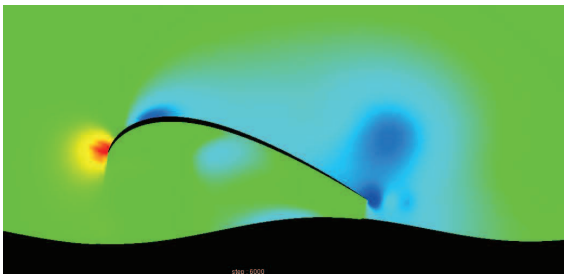

(a) $t$= 6

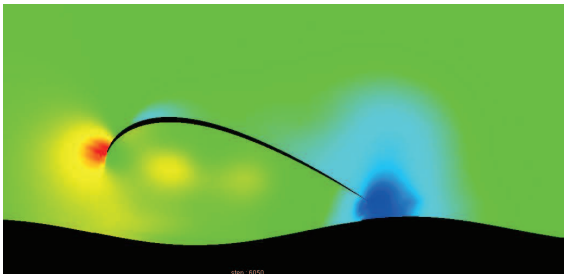

(b) $t$= 6.1

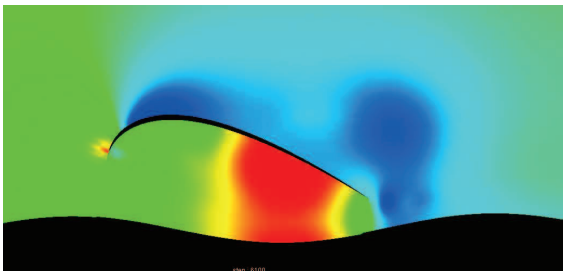

(c) $t$= 6.2

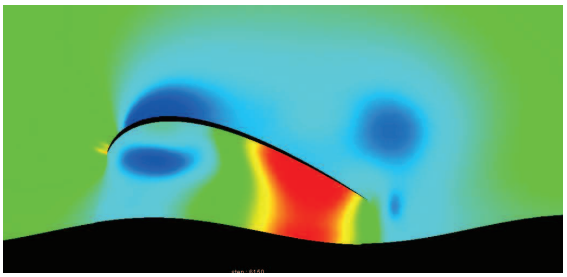

(d) $t$= 6.3

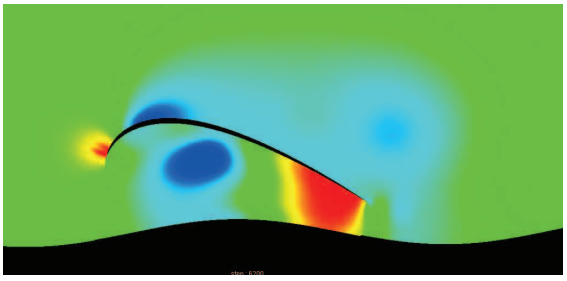

(e) $t$= 6.4

Fig. 15 Pressure field in the center plane

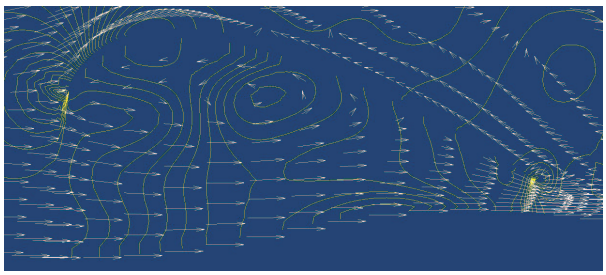

(a) $t$= 6

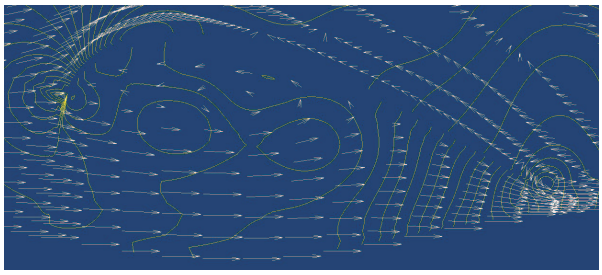

(b) $t$= 6.1

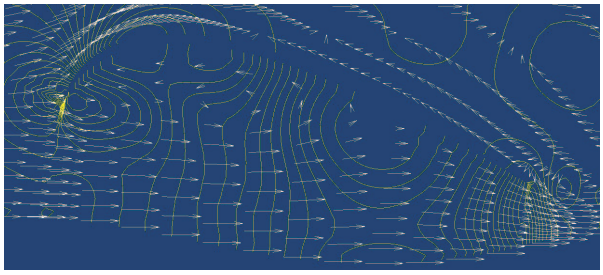

(c) $t$= 6.2

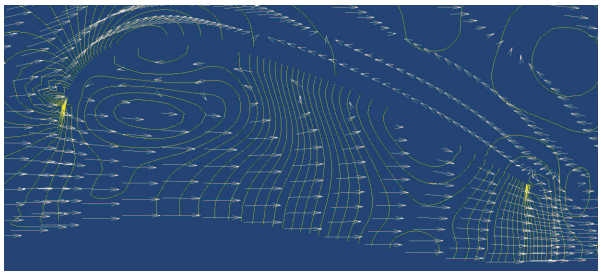

(d) $t$= 6.3

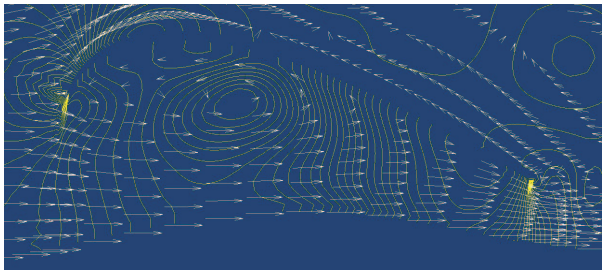

(e) $t$= 6.4

Fig. 16 Pressure contour and velocity in the center plane

Fig.16 shows velocity vectors and isobars at the same time, corresponding to Fig.15. As the distance between the trailing edge and the water surface decreases, the flow velocity near the trailing edge increases.

Fig. 17 and Fig. 18 correspond to Fig. 14 when the traveling wave wavelength is 2C and 4C, and the period of the curve is doubled and quadrupled accordingly compared to the case of C.

It can also be seen that the amplitude of variation decreases as the wavelength increases. Furthermore, the average value of L/D also decreases. Fig. 19 is the result when the amplitude is half (0.025 C) of the case of calculation of Fig. 18 at wavelength 4 C of the traveling wave. Table 3 is the average value and amplitude of L/D for various wavelengths. The value of L/D is about 2 when no wave is present (the result is not shown), but when the wave amplitude is large, the average value becomes large, and when the amplitude is 0.05, it becomes about 2.15.

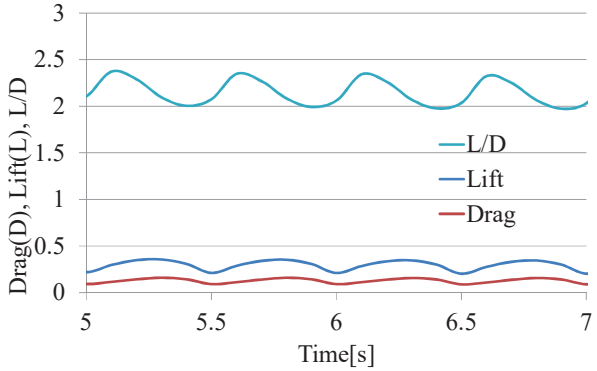


Fig. 17 Corresponding to Fig.14 but wave length is twice

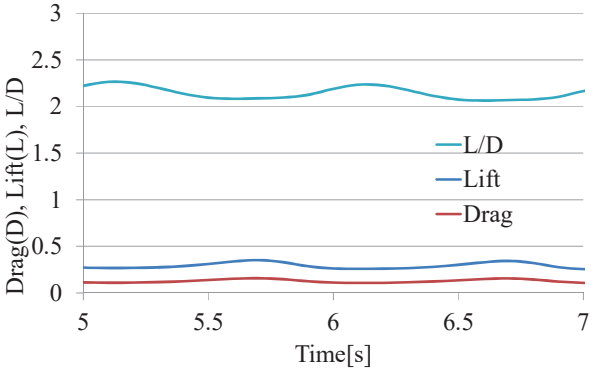


Fig. 18 Corresponding to Fig.14 but wave length is four times

Table 3 Averaged value and amplitude of L/D

| | C | 2C | 4C |
|---|---|---|---|
| averaged L/D | 2.17 | 2.10 | 2.10 |
| amplitude of L/D | 0.71 | 0.35 | 0.15 |

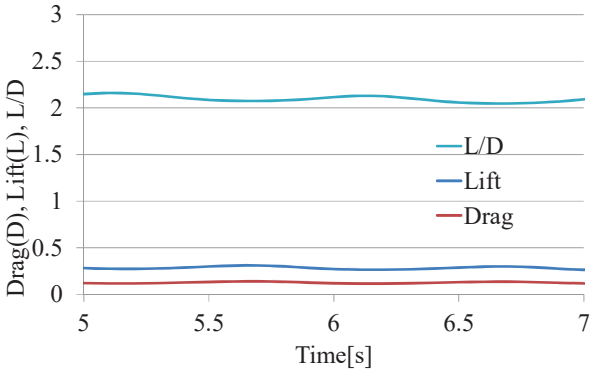


Fig. 19 Corresponding to Fig.18 but amplitude is half

## 5. Summary and future work

In this research, focusing on the flight of WISE, we propose a computational method to estimate flight efficiently and verify it by simulation. As a result, it is found that the closer to the ground and the higher attack angle make the more efficient flight but too large attack angle makes it worse.

We also conduct three-dimensional numerical simulation taking into consideration the influence of waves. At that time, the aircraft is fixed, and waves are made to travel perpendicularly to the aircraft as a one-dimensional traveling wave. Then, the wavelength and amplitude of the wave are changed to investigate in detail the effects on the flow field and the lift effect ratio L/D.

In the future, three-dimensional simulation will be performed under conditions close to the actual condition by changing the incident angle of waves or considering the change of the water surface due to the presence of WISE, and by changing several parameters in order to find out more efficient conditions.

## References

1) Kirill V. Rozhdestvensky, “Wing-in-ground effect veichles”, Progress in Aerospace Sciences, 42, (2006), pp.211-283.
2) Syozo Kubo, Takenori Matsubara, Toshio Matsuoka and Tetuya Kawamura, Fluid Dynamics of Wing-in-Surface Effect Craft “Marine Slider: μ-sky”, Nagare (journal of Japan Society of Fluid Mechanics), (1991), pp.11-23.
3) Syozo Kubo, Toshio Matsuoka and Tetuya Kawamura, Current status of WIG research －Development of μ-sky series－, bulletin of the society of naval architects of Japan, (1990), pp.2-9.
4) Wei Yang, Cheng-Jiong Ying, Zhi-gang Yang, “Aerodynamic study of WIG craft near curved ground”, Journal of Hydrodynamics, 22(5), (2010), pp.371-376.

5) Alexander Nebylov, Vladimir Nebylov, Pierre Fabre, “WIG-CRAFT FLIGHT CONTROL ABOVE THE WAVED SEA”, International Federation of Automatic Control Papers OnLine, 48(9), (2015), pp.102-107.
6) Juhee Lee, “Computational analysis of static height stability and aerodynamics of vehicles with a fuselage, wing and tail in ground effect”, Ocean Engineering, 168, (2018), pp.12-22.
7) N.N.Yanenko, The Method of Fractional Steps, Springer, (1971)

Tetuya Kawamura
Graduate School of Humanities and Sciences, Ochanomizu University
Otsuka 2-1-1, Bunkyo-ku, Tokyo 112-8610, Japan
E-mail: kawamura@is.ocha.ac.jp

Akari Oniiwa
Graduate School of Humanities and Sciences, Ochanomizu University
E-mail: g1420516@is.ocha.ac.jp

Aya Saito
Faculty of Science and Technology, Seikei University
E-mail: saito-aya@st.seikei.ac.jp